THE EUROPEAN
PHYSICAL JOURNAL C

Letter

The new "MUON G-2" result and supersymmetry

Manimala Chakraborti[1,a] , **Sven Heinemeyer**[2,3,4,b], **Ipsita Saha**[5,c]

[1] Astrocent, Nicolaus Copernicus Astronomical Center of the Polish Academy of Sciences, ul. Rektorska 4, 00-614 Warsaw, Poland
[2] Instituto de Física Teórica (UAM/CSIC), Universidad Autónoma de Madrid, Cantoblanco, 28049 Madrid, Spain
[3] Campus of International Excellence UAM+CSIC, Cantoblanco, 28049 Madrid, Spain
[4] Instituto de Física de Cantabria (CSIC-UC), 39005 Santander, Spain
[5] Kavli IPMU (WPI), UTIAS, University of Tokyo, Kashiwa, Chiba 277-8583, Japan

Abstract The electroweak (EW) sector of the Minimal Supersymmetric Standard Model (MSSM), with the lightest neutralino as Dark Matter (DM) candidate, can account for a variety of experimental data. This includes the DM content of the universe, DM direct detection limits, EW SUSY searches at the LHC and in particular the so far persistent $3 - 4\,\sigma$ discrepancy between the experimental result for the anomalous magnetic moment of the muon, $(g - 2)_\mu$, and its Standard Model (SM) prediction. The recently published "MUON G-2" result is within $0.8\,\sigma$ in agreement with the older BNL result on $(g - 2)_\mu$. The combination of the two results was given as $a_\mu^{\mathrm{exp}} = (11659206.1 \pm 4.1) \times 10^{-10}$, yielding a new deviation from the SM prediction of $\Delta a_\mu = (25.1 \pm 5.9) \times 10^{-10}$, corresponding to $4.2\,\sigma$. Using this improved bound we update the results presented in Chakraborti et al. (Eur Phys J C 80(10):984, 2020) and set new upper limits on the allowed parameters space of the EW sector of the MSSM. We find that with the new $(g - 2)_\mu$ result the upper limits on the (next-to-) lightest SUSY particle are in the same ballpark as previously, yielding updated upper limits on these masses of ~ 750 GeV. In this way, a clear target is confirmed for future (HL-)LHC EW searches, as well as for future high-energy e^+e^- colliders, such as the ILC or CLIC.

1 Introduction

Searches for Beyond the Standard Model (BSM) particles are performed directly, such as at the LHC, or indirectly in low-energy experiments and via astrophysical measurements. Among the BSM theories under consideration the Minimal Supersymmetric Standard Model (MSSM) [1–4]

is one of the leading candidates. Supersymmetry (SUSY) predicts two scalar partners for all SM fermions as well as fermionic partners to all SM bosons. Contrary to the case of the SM, in the MSSM two Higgs doublets are required. This results in five physical Higgs bosons instead of the single Higgs boson in the SM. These are the light and heavy $\mathcal{CP}$-even Higgs bosons, h and H, the $\mathcal{CP}$-odd Higgs boson, A, and the charged Higgs bosons, $H^\pm$. The neutral SUSY partners of the (neutral) Higgs and electroweak (EW) gauge bosons gives rise to the four neutralinos, $\tilde{\chi}^0_{1,2,3,4}$. The corresponding charged SUSY partners are the charginos, $\tilde{\chi}^\pm_{1,2}$. The SUSY partners of the SM leptons and quarks are the scalar leptons and quarks (sleptons, squarks), respectively.

In Ref. [5] we performed an analysis taking into account all relevant data for the EW sector of the MSSM, assuming that the lightest SUSY particle (LSP) is given by the lightest neutralino, $\tilde{\chi}^0_1$, that makes up the full Dark Matter (DM) content of the universe [6,7].[1] The experimental results comprised the direct searches at the LHC [9,10], the DM relic abundance [11], the DM direct detection (DD) experiments [12–14] and in particular the (then current) deviation of the anomalous magnetic moment of the muon [15,16].

Three different scenarios were analyzed, classified by the mechanism that brings the LSP relic density into agreement with the measured values. The scenarios differ by the Next-to-LSP (NLSP), where we investigated $\tilde{\chi}^\pm_1$-coannihilation, $\tilde{l}^\pm$-coannihilation with either "left-" or "right-handed" sleptons close in mass to the LSP, Case-L and Case-R, respectively. Using the then current bounds we found upper limits on the LSP masses. While for $\tilde{\chi}^\pm_1$-coannihilation this is ~ 570 GeV, for $\tilde{l}^\pm$-coannihilation Case-L ~ 540 GeV and for Case-R values up to ~ 520 GeV are allowed. Similarly, upper limits to masses of the coannihilating SUSY

a e-mail: mani.chakraborti@gmail.com (corresponding author)

b e-mail: Sven.Heinemeyer@cern.ch

c e-mail: ipsita.saha@ipmu.jp

---

[1] More recently in Ref. [8] we updated the analysis using the DM relic density only as an upper bound.

particles are found as, $m_{\tilde{\chi}_1^\pm} \lesssim 610$ GeV, $m_{\tilde{l}_L} \lesssim 550$ GeV, $m_{\tilde{l}_R} \lesssim 590$ GeV. For the latter, in the $\tilde{l}^\pm$-coannihilation case-R, the upper limit on the lighter $\tilde{\tau}$ is even lower, $m_{\tilde{\tau}_2} \lesssim 530$ GeV. The then current $(g-2)_\mu$ constraint also yields limits on the rest of the EW spectrum, although much loser bounds were found. Previous articles with similar, but in general less advanced studies can be found in Refs. [17–36].

Recently the "MUON G-2" collaboration published the results (referred to as "FNAL" result) of their Run 1 data, which is within $0.8\,\sigma$ in agreement with the older BNL result on $(g-2)_\mu$. We combine the two results, assuming that they are uncorrelated. We analyze the impact of the combination of the Run 1 FNAL data with the previous BNL result on the allowed MSSM parameter space. The results will be discussed in the context of the upcoming searches for EW particles at the HL-LHC. We will also comment on the discovery prospects for these particles at possible future e^+e^- colliders, such as the ILC [37,38] or CLIC [38–41].

2 The model and the experimental constraints

2.1 The model

A detailed description of the EW sector of the MSSM can be found in Ref. [5]. Here we just list the relevant input parameters and masses that are relevant for our analysis. Throughout this paper we assume that all parameters are real, i.e. we have no $\mathcal{CP}$-violation.

The masses and mixings of the charginos and neutralinos are determined by $U(1)_Y$ and $SU(2)_L$ gaugino masses M_1 and M_2, the Higgs mixing parameter μ and $\tan\beta$, the ratio of the two vacuum expectation values (vevs) of the two Higgs doublets of MSSM, $\tan\beta = v_2/v_1$. The four neutralino masses are given as $m_{\tilde{\chi}_1^0} < m_{\tilde{\chi}_2^0} < m_{\tilde{\chi}_3^0} < m_{\tilde{\chi}_4^0}$. Similarly the two chargino-masses are denoted as $m_{\tilde{\chi}_1^\pm} < m_{\tilde{\chi}_2^\pm}$. As argued in Ref. [5] it is sufficient for our analysis to focus on positive values for M_1, M_2 and μ.

For the sleptons, as in Ref. [5], we choose common soft SUSY-breaking parameters for all three generations, $m_{\tilde{l}_L}$ and $m_{\tilde{l}_R}$. We take the trilinear coupling A_l ($l = e, \mu, \tau$) to be zero for all the three generations of leptons. In general we follow the convention that $\tilde{l}_1$ ($\tilde{l}_2$) has the large "left-handed" ("right-handed") component. Besides the symbols equal for all three generations, $m_{\tilde{l}_1}$ and $m_{\tilde{l}_2}$, we also explicitly use the scalar electron, muon and tau masses, $m_{\tilde{e}_{1,2}}$, $m_{\tilde{\mu}_{1,2}}$ and $m_{\tilde{\tau}_{1,2}}$.

Following the stronger experimental limits from the LHC [9,10], we assume that the colored sector of the MSSM is sufficiently heavier than the EW sector, and does not play a role in this analysis. For the Higgs-boson sector we assume that the radiative corrections to the light $\mathcal{CP}$-even Higgs boson (largely originating from the top/stop sec-

tor) yield a value in agreement with the experimental data, $M_h \sim 125$ GeV. This naturally yields stop masses in the TeV range [42,43], in agreement with the above assumption. Concerning the Higgs-boson mass scale, as given by the $\mathcal{CP}$-odd Higgs-boson mass, M_A, we employ the existing experimental bounds from the LHC. In the combination with other data, this results in a non-relevant impact of the heavy Higgs bosons on our analysis, as was discussed in Ref. [5].

2.2 Relevant constraints

The experimental result for $a_\mu := (g-2)_\mu/2$ was so far dominated by the measurements made at the Brookhaven National Laboratory (BNL) [44], resulting in a world average of [45]

$$a_\mu^{\text{exp-BNL}} = (11659209.1 \pm 6.3) \times 10^{-10}, \tag{1}$$

combining statistical and systematic uncertainties. The SM prediction of a_μ is given by [46] (based on Refs. [15,16,47–64]),[2]

$$a_\mu^{\text{SM}} = (11659181.0 \pm 4.3) \times 10^{-10}. \tag{2}$$

Comparing this with the current experimental measurement in Eq. (1) results in a deviation of

$$\Delta a_\mu^{\text{old}} = (28.1 \pm 7.6) \times 10^{-10}, \tag{3}$$

corresponding to a $3.7\,\sigma$ discrepancy.

Recently, the "MUON G-2" collaboration [65] at Fermilab published their Run 1 data [66]

$$a_\mu^{\text{exp-FNAL}} = (11659204.0 \pm 5.4) \times 10^{-10}, \tag{4}$$

being within $0.8\,\sigma$ well compatible with the previous experimental result in Eq. (1). The combined new world average was announced as

$$a_\mu^{\text{exp}} = (11659206.1 \pm 4.1) \times 10^{-10}. \tag{5}$$

Compared with the SM prediction in Eq. (2), one arrives at a new deviation of

$$\Delta a_\mu = (25.1 \pm 5.9) \times 10^{-10}, \tag{6}$$

corresponding to a $4.2\,\sigma$ discrepancy. We use this limit as a cut at the $\pm 2\,\sigma$ level. Here one should note that the new lower $2\,\sigma$ limit is similar to the old one, which leads to the

---

[2] In Ref. [5] a slightly different value was used, with a negligible effect on the results.

expectation that the previously upper bounds, see Ref. [5], are confirmed.

Recently a new lattice calculation for the leading order hadronic vacuum polarization (LO HVP) contribution to a_μ^{SM} [67] has been reported, which, however, was not used in the new theory world average, Eq. (2) [46]. Consequently, we also do not take this result into account, see also the discussions in Refs. [5,67–71]. On the other hand, we are also aware that our conclusions would change substantially if the result presented in [67] turned out to be correct.

In MSSM the main contribution to $(g-2)_\mu$ at the one-loop level comes from diagrams involving $\tilde\chi_1^\pm - \tilde\nu$ and $\tilde\chi_1^0 - \tilde\mu$ loops. In our analysis the MSSM contribution to $(g-2)_\mu$ at two loop order is calculated using GM2Calc [72], implementing two-loop corrections from [73–75] (see also [76,77]).

All other constraints are taken into account exactly as in Ref. [5]. These comprise

- Vacuum stability constraints:
  All points are checked to possess a stable and correct EW vacuum, e.g. avoiding charge and color breaking minima. This check is performed with the public code Evade [78,79].
- Constraints from the LHC:
  All relevant EW SUSY searches are taken into account, mostly via CheckMATE [80–82], where many analysis had to be implemented newly [5].
- Dark matter relic density constraints:
  We use the latest result from Planck [11]. The relic density in the MSSM is evaluated with MicrOMEGAs [83–86].
- Direct detection constraints of Dark matter:
  We employ the constraint on the spin-independent DM scattering cross-section σ_p^{SI} from XENON1T [12] experiment, evaluating the theoretical prediction for σ_p^{SI} using MicrOMEGAs [83–86]. A combination with other DD experiments would yield only very slightly stronger limits, with a negligible impact on our results.

3 Parameter scan

We scan the relevant MSSM parameter space to obtain lower and *upper* limits on the relevant neutralino, chargino and slepton masses. As detailed in Ref. [5] three scan regions cover the relevant parameter space:

(A) bino/wino DM with $\tilde\chi_1^\pm$-coannihilation

$$100 \text{ GeV} \leq M_1 \leq 1 \text{ TeV}, \quad M_1 \leq M_2 \leq 1.1 M_1,$$
$$1.1 M_1 \leq \mu \leq 10 M_1, \quad 5 \leq \tan\beta \leq 60,$$

$$100 \text{ GeV} \leq m_{\tilde l_L} \leq 1 \text{ TeV}, \quad m_{\tilde l_R} = m_{\tilde l_L}. \tag{7}$$

(B) bino DM with $\tilde l^\pm$-coannihilation
(B1) Case-L: SU(2) doublet

$$100 \text{ GeV} \leq M_1 \leq 1 \text{ TeV}, \quad M_1 \leq M_2 \leq 10 M_1,$$
$$1.1 M_1 \leq \mu \leq 10 M_1, \quad 5 \leq \tan\beta \leq 60,$$
$$M_1 \text{ GeV} \leq m_{\tilde l_L} \leq 1.2 M_1, \quad M_1 \leq m_{\tilde l_R} \leq 10 M_1. \tag{8}$$

(B2) Case-R: SU(2) singlet

$$100 \text{ GeV} \leq M_1 \leq 1 \text{ TeV}, \quad M_1 \leq M_2 \leq 10 M_1,$$
$$1.1 M_1 \leq \mu \leq 10 M_1, \quad 5 \leq \tan\beta \leq 60,$$
$$M_1 \text{ GeV} \leq m_{\tilde l_R} \leq 1.2 M_1, \quad M_1 \leq m_{\tilde l_L} \leq 10 M_1. \tag{9}$$

In all three scans we choose flat priors of the parameter space and generate $\mathcal{O}(10^7)$ points. In order to obtain reliable *upper* limits on the various EW SUSY masses, we performed additional smaller scans targeting the highest allowed mass ranges. This will be visible in some of the plots as areas with higher point density. We stress that the point density itself does not have any physical meaning, but only enable us to reliably obtain the upper mass limits.

M_A has also been set to be above the TeV scale. Consequently, we do not include explicitly the possibility of A-pole annihilation, with $M_A \sim 2 m_{\tilde\chi_1^0}$. As we will briefly discuss below the combination of direct heavy Higgs-boson searches with the other experimental requirements constrain this possibility substantially. Similarly, we do not consider h- or Z-pole annihilation (see, e.g., Ref. [36]), as such a light neutralino sector likely overshoots the $(g-2)_\mu$ contribution, see the discussion in Ref. [5].

Analysis flow

The data sample is generated by scanning randomly over the input parameter range mentioned above, using a flat prior for all parameters. We use SuSpect [87] as spectrum and SLHA file generator. The points are required to satisfy the $\tilde\chi_1^\pm$ mass limit from LEP [88]. The SLHA output files from SuSpect are then passed as input to GM2Calc and MicrOMEGAs for the calculation of $(g-2)_\mu$ and the DM observables, respectively. The parameter points that satisfy the new $(g-2)_\mu$ constraint, Eq. (6), the DM relic density and the direct detection constraints and the vacuum stability constraints as checked with Evade are then taken to the final step to be checked against the latest LHC constraints implemented in CheckMATE, as described in detail in Ref. [5]. The branching ratios of the relevant SUSY particles are computed using SDECAY [89] and given as input to CheckMATE.

4 Results

We present the results of the allowed parameter ranges in the three scenarios defined above. We follow the analysis flow as described above and denote the points surviving certain constraints with different colors:

- grey (round): all scan points.
- green (round): all points that are in agreement with $(g - 2)_\mu$, taking into account the new limit as given in Eq. (6).
- blue (triangle): points that additionally give the correct relic density, see Sect. 2.2.
- cyan (diamond): points that additionally pass the DD constraints, see Sect. 2.2.
- red (star): points that additionally pass the LHC constraints, see Sect. 2.2.

4.1 Results in the three DM scenarios

We start in Fig. 1 with the results in the $\tilde{\chi}_1^\pm$-coannihilation scenario. In the $m_{\tilde{\chi}_1^0}$–$m_{\tilde{\chi}_1^\pm}$ plane, shown in the upper left plot, by definition of $\tilde{\chi}_1^\pm$-coannihilation the points are clustered in the diagonal of the plane. One observes a clear upper limit on the (green) points allowed by the new $(g-2)_\mu$ result slightly below 700 GeV, which is similar to the previously obtained one in Ref. [5]. Applying the CDM constraints slightly reduce the upper limit to about 650 GeV, again similar as for the old $(g-2)_\mu$ result. Applying the LHC constraints, corresponding to the "surviving" red points (stars), does not yield a further reduction from above, but cuts always only points in the lower mass range. Thus, the new experimental data set an upper as well as a lower bound, yielding a clear search target for the upcoming LHC runs, and in particular for future e^+e^- colliders, as will be briefly discussed in Sect. 4.2.

The distribution of the lighter slepton mass (where it should be kept in mind that we have chosen the same masses for all three generations, see Sect. 2.1) is presented in the $m_{\tilde{\chi}_1^0}$-$m_{\tilde{l}_1}$ plane, shown in the upper right plot of Fig. 1. The $(g-2)_\mu$ constraint places important constraints in this mass plane, since both types of masses enter into the contributing SUSY diagrams, see Sect. 2.2. The constraint is satisfied in a triangular region with its tip around $(m_{\tilde{\chi}_1^0}, m_{\tilde{l}_1}) \sim$ (700 GeV, 800 GeV), compatible with the old limits. This is slightly reduced to $\sim$ (650 GeV, 700 GeV) when the DM constraints are taken in to account, as can be seen in the distribution of the blue, cyan and red points (triangle/diamond/star). The LHC constraints cut out lower slepton masses, going up to $m_{\tilde{l}_1} \lesssim 500$ GeV, as well as part of the very low $m_{\tilde{\chi}_1^0}$ points nearly independent of $m_{\tilde{l}_1}$. Details on these cuts can be found in Ref. [5]. Clearly visible in the highest $m_{\tilde{\chi}_1^0}$ range as well as in the high $m_{\tilde{l}_1}$ region is the

higher point density due to the additional scan as described in Sect. 3.

We finish our analysis of the $\tilde{\chi}_1^\pm$-coannihilation case with the $m_{\tilde{\chi}_1^0}$-$\tan\beta$ plane presented in the lower plot of Fig. 1. The $(g-2)_\mu$ constraint is fulfilled in a triangular region with largest neutralino masses allowed for the largest $\tan\beta$ values (where we stopped our scan at $\tan\beta = 60$). In agreement with the previous plots, the largest values for the lightest neutralino masses allowed by all the constraints are ~ 650 GeV, compatible with the old $(g-2)_\mu$ limit [5]. The LHC constraints cut out points at low $m_{\tilde{\chi}_1^0}$, nearly independent of $\tan\beta$. Again, the areas with higher point density are plainly visible in the plot (see above). In this plot we also show as a black line the current bound from the LHC searches for heavy neutral Higgs bosons [90] in the channel $pp \to H/A \to \tau\tau$ in the $M_h^{125}(\tilde{\chi})$ benchmark scenario (based on the search data published in Ref. [91] using 139 fb^{-1}).[3] The black line corresponds to $m_{\tilde{\chi}_1^0} = M_A/2$, i.e. roughly to the requirement for A-pole annihilation, where points above the black lines are experimentally excluded. There are very few points passing the current $(g - 2)_\mu$ constraint below the black A-pole line, reaching up to $m_{\tilde{\chi}_1^0} \sim 250$ GeV, for which the A-pole annihilation could provide the correct DM relic density. It can be expected that with the improved limits as given in [91] this possibility is further restricted. These effects make the possibility of A-pole annihilation in this scenario marginal. The final parameter constrained in this scenario is the Higgs-mixing parameter μ. Here in particular, the DD bounds play an important role. Following the analysis in Ref. [5] we find a lower limit of $\mu/M_1 \gtrsim 1.5$ in the $\tilde{\chi}_1^\pm$-coannihilation scenario.

We now turn to the case of $\tilde{l}^\pm$-coannihilation Case-L, as shown in Fig. 2. We start with the $m_{\tilde{\chi}_1^0}$-$m_{\tilde{\mu}_1}$ plane in the upper left plot. By definition of the scenario, the points are located along the diagonal of the plane. The new constraint from $(g - 2)_\mu$ puts an upper bound of ~ 650 GeV on the masses, which is in the same ballpark as for the old $(g - 2)_\mu$ results [5]. Including the DM and LHC constraints, the bound is nearly saturated, i.e. we find an upper limit of ~ 650 GeV.[4] As in the case of $\tilde{\chi}_1^\pm$-coannihilation, the LHC constraints cut away only low mass points. The corresponding implications for the searches at future colliders are briefly discussed in Sect. 4.2.

In upper right plot of Fig. 2 we show the results in the $m_{\tilde{\chi}_1^0}$-$m_{\tilde{\chi}_1^\pm}$ plane. The $(g-2)_\mu$ limits on $m_{\tilde{\chi}_1^0}$ become slightly

---

[3] We thank T. Stefaniak for providing us the limit, using the latest version of `HiggsBounds` [92–96].

[4] This limit is $\sim$ 100 GeV higher than what was found in Ref. [5]. The reason for this increase is the following: a bug in the `GM2calc-v1.5.0` had been detected, which was then fixed in the updated version `v1.7.5`. The bug-fixing leads to a significant deviation in $(g - 2)_\mu$ value in this scenario (but not in the others), which results in a large deviation in the upper limits on the EW masses.

Fig. 1 Results in the $\tilde{\chi}_1^{\pm}$-coannihilation scenario: $m_{\tilde{\chi}_1^0}$–$m_{\tilde{\chi}_1^{\pm}}$ plane (upper left), $m_{\tilde{\chi}_1^0}$–$m_{\tilde{l}_1}$ plane (upper right), $m_{\tilde{\chi}_1^0}$–$\tan\beta$ plane (lower plot); for the color coding: see text
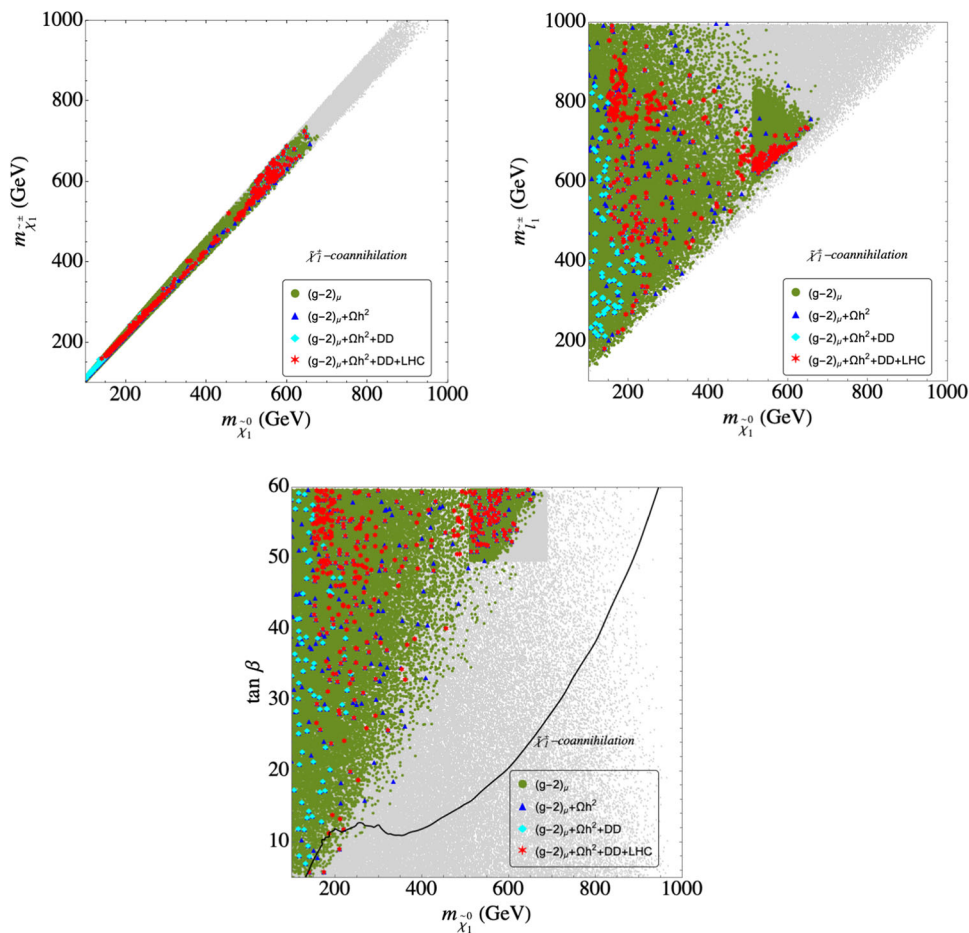

stronger for larger chargino masses, and upper limits on the chargino mass are set at ~ 1.5 TeV. This limit is reduced by ~ 100 GeV by the inclusion of the DM bounds. The LHC limits cut away a lower wedge going up to $m_{\tilde{\chi}_1^{\pm}} \lesssim 600$ GeV. Very low chargino masses are only found in the "accidentally" compressed region of $m_{\tilde{\chi}_1^{\pm}} \approx m_{\tilde{\chi}_1^0}$. Similar to the $\tilde{\chi}_1^{\pm}$-coannihilation scenario, a higher point density can be observed for larger $m_{\tilde{\chi}_1^0}$ due to the additional scanning, see Sect. 3.

The results for the $\tilde{l}^{\pm}$-coannihilation Case-L in the $m_{\tilde{\chi}_1^0}$-$\tan\beta$ plane are presented in the lower plot of Fig. 2. The overall picture is similar to the $\tilde{\chi}_1^{\pm}$-coannihilation case shown above in Fig. 1 i.e. larger LSP masses are allowed for larger $\tan\beta$ values. On the other hand, the combination of small $m_{\tilde{\chi}_1^0}$ and large $\tan\beta$ leads to a *too large* contribution to a_μ^{SUSY} and is thus excluded. As in Fig. 1, we also show the limits from H/A searches at the LHC, where we set (as above) $m_{\tilde{\chi}_1^0} = M_A/2$, i.e. roughly to the requirement for A-pole annihilation, where points above the black lines are experimentally excluded. In this case for the current $(g-2)_\mu$ limit, only very few points passing the $(g-2)_\mu$ constraint "survive" below the black line, i.e. they are potential candidates for A-pole annihilation. The masses reach up to ~ 260 GeV. Together with the already stronger bounds on $H/A \rightarrow \tau\tau$

[91] this does not fully exclude A-pole annihilation, but leaves it as a rather remote possibility. The limits on μ/M_1 (not shown) in the $\tilde{l}^{\pm}$-coannihilation Case-L are again mainly driven by the DD-experiments. Given both CDM constraints and the LHC constraints, the smallest μ/M_1 value we find is 1.7.

We now turn to our third scenario, $\tilde{l}^{\pm}$-coannihilation Case-R, where in the scan we require the "right-handed" sleptons to be close in mass with the LSP. It should be kept in mind that in our notation we do not mass-order the sleptons: for negligible mixing as it is given for selectrons and smuons the "left-handed" ("right-handed") slepton corresponds to $\tilde{l}_1$ ($\tilde{l}_2$). The results are displayed in Fig. 3, where in all four plots the higher point densities due to the additional scans is plainly visible (see Sect. 3). We start our discussion with the $m_{\tilde{\chi}_1^0}$-$m_{\tilde{\mu}_2}$ plane shown in the upper left plot. By definition of the scenario the points are concentrated on the diagonal. The new $(g-2)_\mu$ bound yields an upper limit on the LSP of ~ 700 GeV, in agreement with the previous results [5]. The new $(g-2)_\mu$ bound also places an upper limit on $m_{\tilde{\mu}_2}$ (which is close in mass to the $\tilde{e}_2$ and $\tilde{\tau}_2$) of ~ 800 GeV, again in the same ballpark as for the old $(g-2)_\mu$ result. Including the CDM and LHC constraints, these limits reduce to ~ 650 GeV for the LSP, and correspondingly to ~ 750 GeV

Fig. 2 Results in the
$\tilde{l}^{\pm}$-coannihilation Case-L:
$m_{\tilde{\chi}_1^0}-m_{\tilde{l}_1}$ plane (upper left),
$m_{\tilde{\chi}_1^0}-m_{\tilde{\chi}_1^{\pm}}$ plane (upper right),
$m_{\tilde{\chi}_1^0}-\tan\beta$ plane (lower plot);
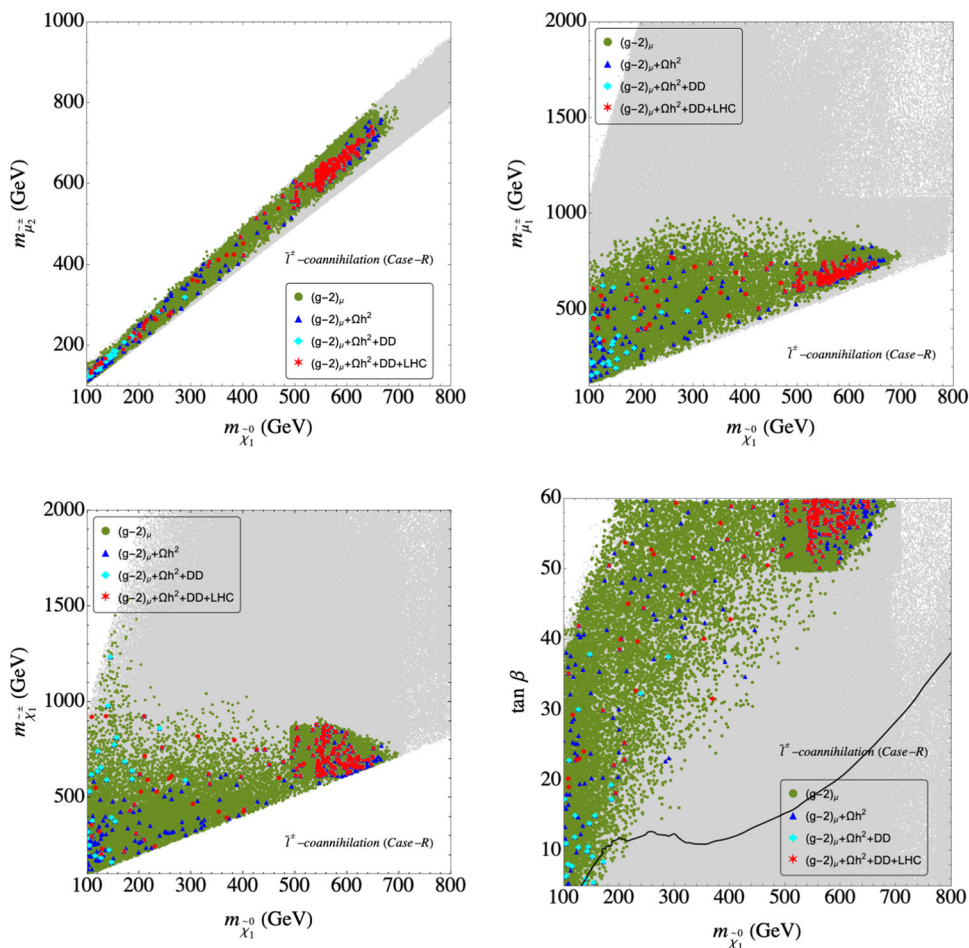for the color coding: see text
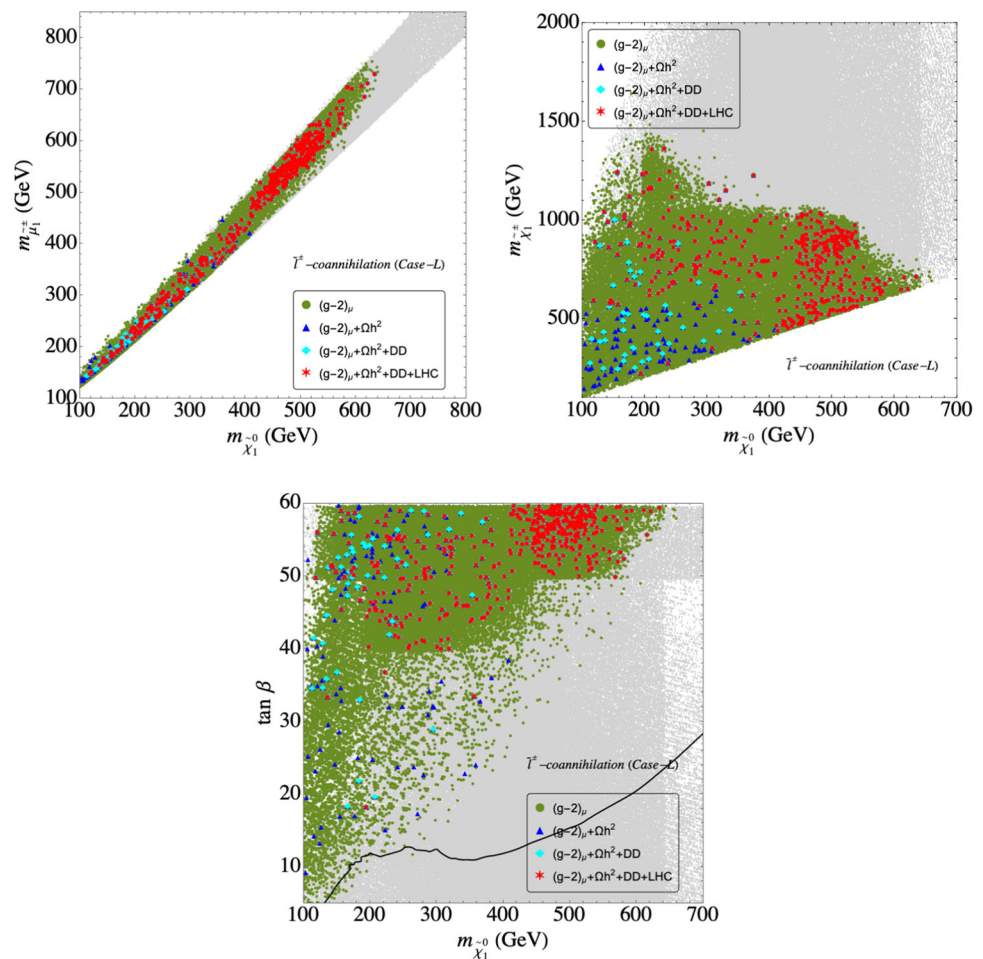
for $m_{\tilde{\mu}_2}$, and ~ 650 GeV for $m_{\tilde{\tau}_2}$. The LHC constraints cut out some, but not all lower-mass points. The upper limits obtained here show a slight increase w.r.t. Ref. [5], which can be attributed to the improved scanning in the higher mass range.

The distribution of the heavier slepton is displayed in the $m_{\tilde{\chi}_1^0}-m_{\tilde{\mu}_1}$ plane in the upper right plot of Fig. 3. Although the "left-handed" sleptons are allowed to be much heavier, the $(g-2)_\mu$ constraint imposes an upper limit of ~ 1000 GeV, about the same as in Ref. [5]. This effect is discussed in detail in Ref. [5]. The DM constraints lead to an upper limit of ~ 850 GeV. The LHC constraints to not yield a further relevant reduction in this case, which cut away only lower mass points and set a lower limit of ~ 400 GeV for the heavier sleptons in the Case-R.

In the lower left plot of Fig. 3 we show the results in the $m_{\tilde{\chi}_1^0}-m_{\tilde{\chi}_1^{\pm}}$ plane. As in the Case-L the $(g-2)_\mu$ limits on $m_{\tilde{\chi}_1^0}$ become slightly stronger for larger chargino masses. The upper limits on the chargino mass, however, are substantially stronger as in the Case-L. They are, also taking into account the DM and LHC constraints reached at ~ 950 GeV using the new $(g-2)_\mu$ result, similar to the limits for the old $(g-2)_\mu$ result [5].

We finish our analysis of the $\tilde{l}^{\pm}$-coannihilation Case-R with the results in the $m_{\tilde{\chi}_1^0}$-$\tan\beta$ plane, presented in the lower right plot of Fig. 3. The overall picture is similar to the previous cases shown above. Larger LSP masses are allowed for larger $\tan\beta$ values. On the other hand, the combination of small $m_{\tilde{\chi}_1^0}$ and very large $\tan\beta$ values, $\tan\beta \gtrsim 40$ leads to stau masses below the LSP mass, which we exclude from the CDM constraints. The LHC searches mainly affect parameter points with $\tan\beta \lesssim 20$. Larger $\tan\beta$ values induce a larger mixing in the third slepton generation, enhancing the probability for charginos to decay via staus and thus evading the LHC constraints. As above we also show the limits from H/A searches at the LHC, where we set $m_{\tilde{\chi}_1^0} = M_A/2$, i.e. roughly to the requirement for A-pole annihilation, where points above the black lines are experimentally excluded. Comparing Case-R and Case-L, in the former case, slightly more points are passing the new $(g-2)_\mu$ constraint below the black line, i.e. are potential candidates for A-pole annihilation. The masses reach only up to ~ 200 GeV, similar to the case of the old $(g-2)_\mu$ result. Together with the already stronger bounds on $H/A \to \tau\tau$ [91] this leaves A-pole annihilation as a quite remote possibility in this scenario.

Fig. 3 Results in the $\tilde{l}^{\pm}$-coannihilation Case-R. $m_{\tilde{\chi}_1^0}-m_{\tilde{l}_2}$ plane (upper left), $m_{\tilde{\chi}_1^0}-m_{\tilde{l}_1}$ plane (upper right), $m_{\tilde{\chi}_1^0}-m_{\tilde{\chi}_1^{\pm}}$ plane (lower left), $m_{\tilde{\chi}_1^0}-\tan\beta$ plane (lower right plot); for the color coding: see text

4.2 Implications for future colliders

In Ref. [5] we had evaluated the prospects for EW searches at the HL-LHC [97] and at a hypothetical future e^+e^- collider such as ILC [37,38] or CLIC [38–41].

The prospects for BSM phenomenology at the HL-LHC have been summarized in [97] for a 14 TeV run with 3 ab^{-1} of integrated luminosity. For the direct production of charginos and neutralinos through EW interaction, the projected 95% exclusion reach as well as a 5σ discovery reach have been presented. Following the discussion in Ref. [5] we conclude that via these searches the updated $(g-2)_\mu$ limit together with DM constraints can conclusively probe "almost" the entire allowed parameter region of $\tilde{l}^{\pm}$-coannihilation Case-R scenario and a significant part of the same parameter space for Case-L scenario at the HL-LHC. On the other hand, the analysis for compressed higgsino-like spectra at the HL-LHC, see the discussion in Ref. [8], may exclude

The limits on μ/M_1 (not shown) in the $\tilde{l}^{\pm}$-coannihilation Case-R are as before mainly driven by the DD-experiments. Given both CDM constraints and the LHC constraints, the smallest μ/M_1 value we find is 1.7.

$m_{\tilde{\chi}_2^0} \sim m_{\tilde{\chi}_1^{\pm}} \sim 350$ GeV with mass gap as low as 2 GeV for $m_{\tilde{\chi}_1^{\pm}}$ around 100 GeV. Hence, a substantial parameter region can be curbed for the $\tilde{\chi}_1^{\pm}$-coannihilation case in the absence of a signal in the compressed scenario analysis with soft leptons at the final state. However, higher energies in pp collisions or an e^+e^- collider with energies up to $\sqrt{s} \sim 1.5$ TeV will be needed to probe this scenario completely [98,99]).

Direct production of EW particles at e^+e^- colliders clearly profits from a higher center-of-mass energy, $\sqrt{s}$. Consequently, we focus here on the two proposals for linear e^+e^- colliders, ILC [37,38] and CLIC [38–41], which can reach energies up to 1 TeV, and 3 TeV, respectively. In Ref. [5] we had evaluated the cross-sections for the various SUSY pair production modes (based on Refs. [100,101]) for the energies currently foreseen in the run plans of the two colliders.

Taking into account the results for the cross-sections evaluated in Ref. [5], one can conclude that the new accuracy on $(g-2)_\mu$, yielding similar upper limits on EW SUSY particles, guarantees the discovery at the higher-energy stages of the ILC and/or CLIC. This holds in particular for the LSP and the NLSP. The improved $(g-2)_\mu$ constraint, confirming the deviation of $a_\mu^{\exp}$ from the SM prediction, clearly strengthens the case for future e^+e^- colliders.

As discussed in Sect. 3 we have not considered the possibility of Z or h pole annihilation to find agreement of the relic DM density with the other experimental measurements. However, it should be noted that in this context an LSP with $M_1 \sim m_{\tilde{\chi}_1^0} \sim M_Z/2$ or $\sim M_h/2$ would yield a detectable cross-section $e^+e^- \rightarrow \tilde{\chi}_1^0 \tilde{\chi}_1^0 \gamma$ in any future high-energy e^+e^- collider. Furthermore, depending on the values of M_2 and μ, this scenario likely yields other clearly detectable EW-SUSY production cross-sections at future e^+e^- colliders. We leave this possibility for future studies.

On the other hand, the possibility of A-pole annihilation was briefly discussed for all three scenarios. While it appears a rather remote possibility, it cannot be fully excluded by our analysis. However, overall an upper limit for this scenario on $m_{\tilde{\chi}_1^0}$ of ~ 260 GeV can be set. While not as low as in the case of Z or h-pole annihilation, this would still offer good prospects for future e^+e^- colliders. We leave also this possibility for future studies.

5 Conclusions

The electroweak (EW) sector of the MSSM, consisting of charginos, neutralinos and scalar leptons can account for a variety of experimental data: the CDM relic abundance with the lightest neutralino, $\tilde{\chi}_1^0$ as LSP, the bounds from DD experiments as well as from direct searches at the LHC. Most importantly, the EW sector of the MSSM can account for the long-standing discrepancy of $(g-2)_\mu$. The new result for the Run 1 data of the "MUON G-2" experiment confirmed the deviation from the SM prediction found previously.

Under the assumption that the previous experimental result on $(g-2)_\mu$ is uncorrelated with the new "MUON G-2" result we combined the data and obtained a new deviation from the SM prediction of $\Delta a_\mu = (25.1 \pm 5.9) \times 10^{-10}$, corresponding to a $4.2\,\sigma$ discrepancy. We used this limit as a cut at the $\pm 2\,\sigma$ level.

In this paper, under the assumption that the $\tilde{\chi}_1^0$ provides the full DM relic abundance we analyzed which mass ranges of neutralinos, charginos and sleptons are in agreement with all relevant experimental data: the new limit for $(g-2)_\mu$, the relic density bounds, the DD experimental bounds, as well as the LHC searches for EW SUSY particles. These results present an update of Ref. [5], where the previous $(g-2)_\mu$ result had been used (as well as a hypothetical "MUON G-2" result).

We analyzed three scenarios, depending on the mechanism that brings the relic density in agreement with the experimental data: $\tilde{\chi}_1^\pm$-coannihilation, $\tilde{l}^\pm$-coannihilation with the mass of the "left-handed" ("right-handed") slepton close to $m_{\tilde{\chi}_1^0}$, Case-L (Case-R). We find in all three cases a clear upper limit on $m_{\tilde{\chi}_1^0}$. We find that the upper limits on the LSP mass are roughly reproduced to be of ~ 650 GeV in all three scenarios, confirming the collider targets w.r.t. the old $(g-2)_\mu$. Similarly, the upper limits on the NLSP masses are confirmed to about 750 GeV in the three cases that we have explored, again compatible with the previous $(g-2)_\mu$ result.

For the HL-LHC we have briefly discussed the prospects to cover the parameter regions that are preferred by the new $(g-2)_\mu$ result. In particular the $\tilde{l}^\pm$-coannihilation Case-R can be conclusively tested at the HL-LHC, while the other scenarios are only partially covered. Concerning future high(er) energy e^+e^- colliders, ILC and CLIC, one can conclude that the new accuracy on $(g-2)_\mu$ confirms the upper limits on EW SUSY, and it can be expected that at least some particles can be discovered at the higher-energy stages of the ILC and/or CLIC. This holds in particular for the LSP and the NLSP. Therefore, the new $(g-2)_\mu$ constraint, confirming the deviation of a_μ^{exp} from the SM prediction, strongly motivates the need of future e^+e^- colliders.

References

1. H. Nilles, Phys. Rep. **110**, 1 (1984)
2. R. Barbieri, Riv. Nuovo Cim. **11**, 1 (1988)
3. H. Haber, G. Kane, Phys. Rep. **117**, 75 (1985)
4. J. Gunion, H. Haber, Nucl. Phys. B **272**, 1 (1986)
5. M. Chakraborti, S. Heinemeyer, I. Saha, Eur. Phys. J. C **80**(10), 984 (2020). arXiv:2006.15157 [hep-ph]
6. H. Goldberg, Phys. Rev. Lett. **50**, 1419 (1983)

7. J. Ellis, J. Hagelin, D. Nanopoulos, K. Olive, M. Srednicki, Nucl. Phys. B **238**, 453 (1984)

8. M. Chakraborti, S. Heinemeyer, I. Saha, Improved $(g-2)_\mu$ measurements and wino/higgsino dark matter. Eur. Phys. J. C **81**(12), 1069 (2021). https://doi.org/10.1140/epjc/s10052-021-09814-1. arXiv:2103.13403 [hep-ph]

9. See: https://twiki.cern.ch/twiki/bin/view/AtlasPublic/SupersymmetryPublicResults

10. See: https://twiki.cern.ch/twiki/bin/view/CMSPublic/PhysicsResultsSUS

11. N. Aghanim et al. (Planck), Astron. Astrophys. **641**, A6 (2020). arXiv:1807.06209 [astro-ph.CO] [Erratum: Astron. Astrophys. **652**, C4 (2021)]

12. E. Aprile et al. (XENON Collaboration), Phys. Rev. Lett. **121**(11), 111302 (2018). arXiv:1805.12562 [astro-ph.CO]

13. D.S. Akerib et al. (LUX Collaboration), Phys. Rev. Lett. **118**(2), 021303 (2017). arXiv:1608.07648 [astro-ph.CO]

14. X. Cui et al. (PandaX-II Collaboration), Phys. Rev. Lett. **119**(18), 181302 (2017). arXiv:1708.06917 [astro-ph.CO]

15. A. Keshavarzi, D. Nomura, T. Teubner, Phys. Rev. D **101**(1), 014029 (2020). arXiv:1911.00367 [hep-ph]

16. M. Davier, A. Hoecker, B. Malaescu, Z. Zhang, Eur. Phys. J. C **80**(3), 241 (2020). arXiv:1908.00921 [hep-ph]

17. A. Bharucha, S. Heinemeyer, F. von der Pahlen, Eur. Phys. J. C **73**(11), 2629 (2013). arXiv:1307.4237 [hep-ph]

18. A. Fowlie, K. Kowalska, L. Roszkowski, E.M. Sessolo, Y.L.S. Tsai, Phys. Rev. D **88**, 055012 (2013). arXiv:1306.1567 [hep-ph]

19. T. Han, S. Padhi, S. Su, Phys. Rev. D **88**(11), 115010 (2013). arXiv:1309.5966 [hep-ph]

20. K. Kowalska, L. Roszkowski, E.M. Sessolo, A.J. Williams, JHEP **06**, 020 (2015). arXiv:1503.08219 [hep-ph]

21. A. Choudhury, S. Mondal, Phys. Rev. D **94**(5), 055024 (2016). arXiv:1603.05502 [hep-ph]

22. A. Datta, N. Ganguly, S. Poddar, Phys. Lett. B **763**, 213–217 (2016). arXiv:1606.04391 [hep-ph]

23. M. Chakraborti, A. Datta, N. Ganguly, S. Poddar, JHEP **1711**, 117 (2017). arXiv:1707.04410 [hep-ph]

24. K. Hagiwara, K. Ma, S. Mukhopadhyay, Phys. Rev. D **97**(5), 055035 (2018). arXiv:1706.09313 [hep-ph]

25. T.T. Yanagida, W. Yin, N. Yokozaki, JHEP **06**, 154 (2020). arXiv:2001.02672 [hep-ph]

26. W. Yin, N. Yokozaki, Phys. Lett. B **762**, 72–79 (2016). arXiv:1607.05705 [hep-ph]

27. T.T. Yanagida, W. Yin, N. Yokozaki, JHEP **09**, 086 (2016). arXiv:1608.06618 [hep-ph]

28. M. Chakraborti, U. Chattopadhyay, S. Poddar, JHEP **1709**, 064 (2017). arXiv:1702.03954 [hep-ph]

29. E.A. Bagnaschi et al., Eur. Phys. J. C **75**, 500 (2015). arXiv:1508.01173 [hep-ph]

30. A. Datta, N. Ganguly, JHEP **1801**, 103 (2019). arXiv:1809.05129 [hep-ph]

31. P. Cox, C. Han, T.T. Yanagida, Phys. Rev. D **98**(5), 055015 (2018). arXiv:1805.02802 [hep-ph]

32. M. Abdughani, K. Hikasa, L. Wu, J.M. Yang, J. Zhao, JHEP **1911**, 095 (2019). arXiv:1909.07792 [hep-ph]

33. M. Endo, K. Hamaguchi, S. Iwamoto, T. Kitahara, JHEP **2004**, 165 (2020). arXiv:2001.11025 [hep-ph]

34. G. Pozzo, Y. Zhang, Phys. Lett. B **789**, 582–591 (2019). arXiv:1807.01476 [hep-ph]

35. P. Athron et al. (GAMBIT), Eur. Phys. J. C **79**(5), 395 (2019). arXiv:1809.02097 [hep-ph]

36. M. Carena, J. Osborne, N.R. Shah, C.E.M. Wagner, Phys. Rev. D **98**(11), 115010 (2018). arXiv:1809.11082 [hep-ph]

37. H. Baer et al., *The International Linear Collider Technical Design Report—Volume 2: Physics*. arXiv:1306.6352 [hep-ph]

38. G. Moortgat-Pick et al., Eur. Phys. J. C **75**(8), 371 (2015). arXiv:1504.01726 [hep-ph]

39. L. Linssen, A. Miyamoto, M. Stanitzki, H. Weerts, arXiv:1202.5940 [physics.ins-det]

40. H. Abramowicz et al. (CLIC Detector and Physics Study Collaboration), arXiv:1307.5288 [hep-ex]

41. P. Burrows et al. (CLICdp and CLIC Collaborations), CERN Yellow Rep. Monogr. **1802**, 1 (2018). arXiv:1812.06018 [physics.acc-ph]

42. E. Bagnaschi et al., Eur. Phys. J. C **78**(3), 256 (2018). arXiv:1710.11091 [hep-ph]

43. P. Slavich, S. Heinemeyer, E. Bagnaschi, H. Bahl, M. Goodsell, H.E. Haber, T. Hahn, R. Harlander, W. Hollik, G. Lee et al., Eur. Phys. J. C **81**(5), 450 (2021). arXiv:2012.15629 [hep-ph]

44. G.W. Bennett et al. (Muon g-2 Collaboration), Phys. Rev. D **73**, 072003 (2006). arXiv:hep-ex/0602035

45. M. Tanabashi et al. (Particle Data Group), Phys. Rev. D **98**(3), 030001 (2018)

46. T. Aoyama, N. Asmussen, M. Benayoun, J. Bijnens, T. Blum, M. Bruno, I. Caprini, C.M. Carloni Calame, M. Cè, G. Colangelo, et al. The anomalous magnetic moment of the muon in the Standard Model. Phys. Rept. **887**, 1–166 (2020). https://doi.org/10.1016/j.physrep.2020.07.006. arXiv:2006.04822 [hep-ph]

47. T. Aoyama, M. Hayakawa, T. Kinoshita, M. Nio, Phys. Rev. Lett. **109**, 111808 (2012). arXiv:1205.5370 [hep-ph]

48. T. Aoyama, T. Kinoshita, M. Nio, Atoms **7**(1), 28 (2019)

49. A. Czarnecki, W.J. Marciano, A. Vainshtein, Phys. Rev. D **67**, 073006 (2003). arXiv:hep-ph/0212229

50. C. Gnendiger, D. Stöckinger, H. Stöckinger-Kim, Phys. Rev. D **88**, 053005 (2013). arXiv:1306.5546 [hep-ph]

51. M. Davier, A. Hoecker, B. Malaescu, Z. Zhang, Eur. Phys. J. C **77**(12), 827 (2017). arXiv:1706.09436 [hep-ph]

52. A. Keshavarzi, D. Nomura, T. Teubner, Phys. Rev. D **97**(11), 114025 (2018). arXiv:1802.02995 [hep-ph]

53. G. Colangelo, M. Hoferichter, P. Stoffer, JHEP **02**, 006 (2019). arXiv:1810.00007 [hep-ph]

54. M. Hoferichter, B.L. Hoid, B. Kubis, JHEP **08**, 137 (2019). arXiv:1907.01556 [hep-ph]

55. A. Kurz, T. Liu, P. Marquard, M. Steinhauser, Phys. Lett. B **734**, 144–147 (2014). arXiv:1403.6400 [hep-ph]

56. K. Melnikov, A. Vainshtein, Phys. Rev. D **70**, 113006 (2004). arXiv:hep-ph/0312226

57. P. Masjuan, P. Sanchez-Puertas, Phys. Rev. D **95**(5), 054026 (2017). arXiv:1701.05829 [hep-ph]

58. G. Colangelo, M. Hoferichter, M. Procura, P. Stoffer, JHEP **04**, 161 (2017). arXiv:1702.07347 [hep-ph]

59. M. Hoferichter, B.L. Hoid, B. Kubis, S. Leupold, S.P. Schneider, JHEP **10**, 141 (2018). arXiv:1808.04823 [hep-ph]

60. A. Gérardin, H.B. Meyer, A. Nyffeler, Phys. Rev. D **100**(3), 034520 (2019). arXiv:1903.09471 [hep-lat]

61. J. Bijnens, N. Hermansson-Truedsson, A. Rodríguez-Sánchez, Phys. Lett. B **798**, 134994 (2019). arXiv:1908.03331 [hep-ph]

62. G. Colangelo, F. Hagelstein, M. Hoferichter, L. Laub, P. Stoffer, JHEP **03**, 101 (2020). arXiv:1910.13432 [hep-ph]

63. T. Blum, N. Christ, M. Hayakawa, T. Izubuchi, L. Jin, C. Jung, C. Lehner, Phys. Rev. Lett. **124**(13), 132002 (2020). arXiv:1911.08123 [hep-lat]

64. G. Colangelo, M. Hoferichter, A. Nyffeler, M. Passera, P. Stoffer, Phys. Lett. B **735**, 90–91 (2014). arXiv:1403.7512 [hep-ph]

65. J. Grange et al. (Muon g-2 Collaboration), arXiv:1501.06858 [physics.ins-det]

66. C. Polly ("MUON G-2" Collaboration), Talk: first results from the muon $g-2$ experiment at Fermilab. Fermilab, April 7, 2021. See https://news.fnal.gov/2021/04/first-results-from-fermilabs-muon-g-2-experiment-strengthen-evidence-of-new-physics

67. S. Borsanyi, Z. Fodor, J.N. Guenther, C. Hoelbling, S.D. Katz, L. Lellouch, T. Lippert, K. Miura, L. Parato, K.K. Szabo, et al. Leading hadronic contribution to the muon magnetic moment from lattice QCD. Nature **593**(7857), 51–55 (2021). https://doi.org/10.1038/s41586-021-03418-1. arXiv:2002.12347 [hep-lat]

68. C. Lehner, A.S. Meyer, Consistency of hadronic vacuum polarization between lattice QCD and the R-ratio. Phys. Rev. D **101**, 074515 (2020). https://doi.org/10.1103/PhysRevD.101.074515, arXiv:2003.04177 [hep-lat]

69. A. Crivellin, M. Hoferichter, C.A. Manzari, M. Montull, Hadronic vacuum polarization: $(g - 2)_\mu$ versus global electroweak fits. Phys. Rev. Lett. **125**(9), 091801 (2020). https://doi.org/10.1103/PhysRevLett.125.091801. arXiv:2003.04886 [hep-ph]

70. A. Keshavarzi, W.J. Marciano, M. Passera, A. Sirlin, Muon $g - 2$ and $\Delta\alpha$ connection. Phys. Rev. D **102**(3), 033002 (2020). https://doi.org/10.1103/PhysRevD.102.033002. arXiv:2006.12666 [hep-ph]

71. E. de Rafael, Constraints between $\Delta\alpha_{\mathrm{had}}(M_Z^2)$ and $(g_\mu - 2)_{\mathrm{HVP}}$. Phys. Rev. D **102**(5), 056025 (2020). https://doi.org/10.1103/PhysRevD.102.056025. arXiv:2006.13880 [hep-ph]

72. P. Athron et al., Eur. Phys. J. C **76**(2), 62 (2016). arXiv:1510.08071 [hep-ph]

73. P. von Weitershausen, M. Schafer, H. Stockinger-Kim, D. Stockinger, Phys. Rev. D **81**, 093004 (2010). arXiv:1003.5820 [hep-ph]

74. H. Fargnoli, C. Gnendiger, S. Paßehr, D. Stöckinger, H. Stöckinger-Kim, JHEP **1402**, 070 (2014). arXiv:1311.1775 [hep-ph]

75. M. Bach, J.H. Park, D. Stöckinger, H. Stöckinger-Kim, JHEP **1510**, 026 (2015). arXiv:1504.05500 [hep-ph]

76. S. Heinemeyer, D. Stockinger, G. Weiglein, Nucl. Phys. B **690**, 62–80 (2004). arXiv:hep-ph/0312264

77. S. Heinemeyer, D. Stockinger, G. Weiglein, Nucl. Phys. B **699**, 103–123 (2004). arXiv:hep-ph/0405255

78. W.G. Hollik, G. Weiglein, J. Wittbrodt, JHEP **03**, 109 (2019). arXiv:1812.04644 [hep-ph]

79. P.M. Ferreira, M. Mühlleitner, R. Santos, G. Weiglein, J. Wittbrodt, JHEP **09**, 006 (2019). arXiv:1905.10234 [hep-ph]

80. M. Drees, H. Dreiner, D. Schmeier, J. Tattersall, J.S. Kim, Comput. Phys. Commun. **187**, 227–265 (2015). arXiv:1312.2591 [hep-ph]

81. J.S. Kim, D. Schmeier, J. Tattersall, K. Rolbiecki, Comput. Phys. Commun. **196**, 535–562 (2015). arXiv:1503.01123 [hep-ph]

82. D. Dercks, N. Desai, J.S. Kim, K. Rolbiecki, J. Tattersall, T. Weber, Comput. Phys. Commun. **221**, 383–418 (2017). arXiv:1611.09856 [hep-ph]

83. G. Belanger, F. Boudjema, A. Pukhov, A. Semenov, Comput. Phys. Commun. **149**, 103–120 (2002). arXiv:hep-ph/0112278

84. G. Belanger, F. Boudjema, A. Pukhov, A. Semenov, Comput. Phys. Commun. **176**, 367–382 (2007). arXiv:hep-ph/0607059

85. G. Belanger, F. Boudjema, A. Pukhov, A. Semenov, Comput. Phys. Commun. **177**, 894–895 (2007). [84]

86. G. Belanger, F. Boudjema, A. Pukhov, A. Semenov, micrOMEGAs_3: A program for calculating dark matter observables. Comput. Phys. Commun. **185**, 960–985 (2014). https://doi.org/10.1016/j.cpc.2013.10.016. arXiv:1305.0237 [hep-ph]

87. A. Djouadi, J.L. Kneur, G. Moultaka, Comput. Phys. Commun. **176**, 426 (2007). arXiv:hep-ph/0211331

88. Joint LEP2 SUSY Working Group, the ALEPH, DELPHI, L3 and OPAL Collaborations. http://lepsusy.web.cern.ch/lepsusy/

89. M. Muhlleitner, A. Djouadi, Y. Mambrini, Comput. Phys. Commun. **168**, 46 (2005). arXiv:hep-ph/0311167

90. E. Bagnaschi et al., Eur. Phys. J. C **79**(7), 617 (2019). arXiv:1808.07542 [hep-ph]

91. G. Aad et al. [ATLAS], Search for heavy Higgs bosons decaying into two tau leptons with the ATLAS detector using pp collisions at $\sqrt{s}$ = 13 TeV. Phys. Rev. Lett. **125**(5), 051801 (2020). https://doi.org/10.1103/PhysRevLett.125.051801. arXiv:2002.12223 [hep-ex]

92. P. Bechtle, O. Brein, S. Heinemeyer, G. Weiglein, K.E. Williams, Comput. Phys. Commun. **181**, 138–167 (2010). arXiv:0811.4169 [hep-ph]

93. P. Bechtle, O. Brein, S. Heinemeyer, G. Weiglein, K.E. Williams, Comput. Phys. Commun. **182**, 2605–2631 (2011). arXiv:1102.1898 [hep-ph]

94. P. Bechtle, O. Brein, S. Heinemeyer, O. Stål, T. Stefaniak, G. Weiglein, K.E. Williams, Eur. Phys. J. C **74**(3), 2693 (2014). arXiv:1311.0055 [hep-ph]

95. P. Bechtle, S. Heinemeyer, O. Stål, T. Stefaniak, G. Weiglein, Eur. Phys. J. C **75**(9), 421 (2015). arXiv:1507.06706 [hep-ph]

96. P. Bechtle, D. Dercks, S. Heinemeyer, T. Klingl, T. Stefaniak, G. Weiglein, J. Wittbrodt, Eur. Phys. J. C **80**(12), 1211 (2020). arXiv:2006.06007 [hep-ph]

97. X. Cid Vidal et al., CERN Yellow Rep. Monogr. **7**, 585–865 (2019). arXiv:1812.07831 [hep-ph]

98. R.K. Ellis et al., arXiv:1910.11775 [hep-ex]

99. M. Berggren, arXiv:2003.12391 [hep-ph]

100. S. Heinemeyer, C. Schappacher, Eur. Phys. J. C **77**(9), 649 (2017). arXiv:1704.07627 [hep-ph]

101. S. Heinemeyer, C. Schappacher, Eur. Phys. J. C **78**(7), 536 (2018). arXiv:1803.10645 [hep-ph]